Exciton diffusion and optical interference in organic donor–acceptor photovoltaic cells

Thomas Stübinger, and Wolfgang Brütting

View Online   Export Citation

ARTICLES YOU MAY BE INTERESTED IN

AIP
Publishing

Exciton diffusion and optical interference in organic donor−acceptor photovoltaic cells

Thomas Stübinger[a] and Wolfgang Brütting
Experimental Physics II, University of Bayreuth, 95440 Bayreuth, Germany

The influence of the organic layer thickness on short-circuit photocurrent spectra and efficiency is investigated in heterojunction photovoltaic cells with the electron donor materials poly(*p*-phenylenevinylene) (PPV) and Cu-phthalocyanine (CuPc), respectively, together with C_{60} as electron acceptor material. The main process of photocurrent generation after light absorption, exciton generation, and exciton diffusion in the bulk of the absorbing material is given by the exciton dissociation at the donor−acceptor interface. We determined a strong dependence of the optimum layer thickness of the absorbing material on the exciton diffusion length by systematically varying the layer thickness of the electron donor material. Additionally, a significant photocurrent contribution occurred due to light absorption and exciton generation in the C_{60} layer with a subsequent hole transfer to PPV, respectively, CuPc at the dissociation interface. Using a simple rate equation for the exciton density we estimated the exciton diffusion lengths from the measured photocurrent spectra yielding (12 ± 3) nm in PPV and (68 ± 20) nm in CuPc. By systematically varying the layer thickness of the C_{60} layer we were able to investigate an optical interference effect due to a superposition of the incident with backreflected light from the Al electrode. Therefore both the layer thickness of the donor and of the acceptor layer significantly influence not only the photocurrent spectra but also the efficiencies of these heterolayer devices. With optimized donor and acceptor layer thicknesses power conversion efficiencies of about 0.5% under white light illumination were obtained. © *2001 American Institute of Physics.* [DOI: 10.1063/1.1394920]

I. INTRODUCTION

Organic thin film photovoltaic devices based on conjugated polymers and conjugated low molecular-weight materials with high absorption coefficients are promising candidates for efficient photon-to-current conversion.[1–16] While photovoltaic cells consisting of a single layer of a conjugated polymer in general exhibit low efficiency of energy conversion,[4–7] blends[8,12,17,18] and heterojunctions[1,3,10,19,20] with materials having high electron affinity considerably enhance not only the photon-to-current efficiency but also the more important power conversion efficiency.

The primary step of photocurrent generation in organic thin film photovoltaic devices is due to the creation of strongly bound excitons after light absorption in the active absorbing parts of the devices with exciton binding energies E_B of some tenths of an eV (e.g., $E_B = 0.4$ eV for excitons in the conjugated polymer PPV).[6,21] The generation of separated charges occurs as a result of dissociation of these strongly bound excitons by interaction with interfaces, impurities, or defects, or in high electric fields. Competing pathways are radiative and nonradiative recombination, the former being important especially in materials with high photoluminescence efficiency. A very efficient exciton dissociation process has been found by Sariciftci *et al.*[22] in the ultrafast photoinduced electron transfer from excited conjugated polymers to the lowest unoccupied molecular orbital (LUMO) of the Buckminsterfullerene C_{60}. This ultrafast

electron transfer takes place on a subpicosecond time scale,[3,22–26] which is about three orders of magnitude faster than typical radiative lifetimes of a few nanoseconds. Therefore the main dissociation process in heterojunction cells takes place only at or in the vicinity of the donor−acceptor interface. Dissociation processes in the bulk region of the materials can be neglected. The fact that photoluminescence quenching occurs within a range of 5 nm in a conjugated polymer in contact with an additional C_{60} layer[27] confirms the assumption that exciton dissociation is sharply located at the donor−acceptor interface if the exciton diffusion length is small like in PPV.

The generation of excitons is strongly dependent on the distribution of the light intensity inside the absorbing material, which consequently influences the photovoltaic properties of the cells.[20] Additionally, reflections at the metal/organic interface leading to optical interference effects can significantly affect the distribution of the light intensity inside the device. Therefore the layer thicknesses of both the donor and the acceptor layers are important parameters which influence the quantum efficiencies of the cells, also because of the low charge carrier mobilities (<1 cm^2/V s) and low conductivities in the respective materials as compared to inorganic semiconductors.[28–31]

Different models have been developed to describe the photovoltaic action spectra.[4,32–36] Harrison *et al.*[34] give a thorough description of some of these models. Common to all of them is the assumption that the intensity of the optical electric field shows an exponential decrease along the direction of propagation inside the device structure, reflections

[a]Electronic mail: thomas.stuebinger@uni-bayreuth.de
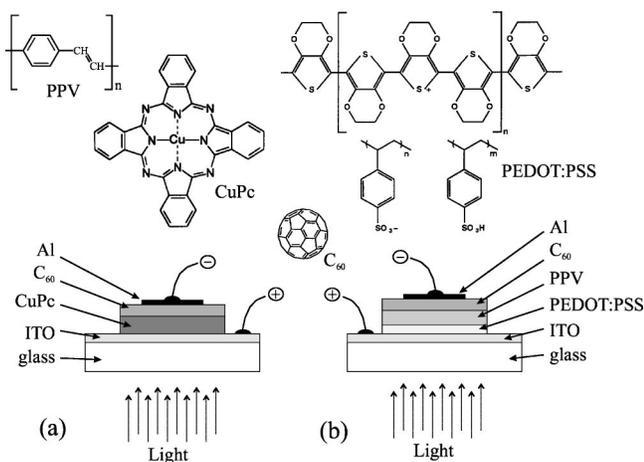
FIG. 1. Chemical structure of poly(p-phenylenevinylene) (PPV), Cu-phthalocyanine (CuPc), poly(3,4-ethylenedioxythiophene): poly(styrene-sulfonate) (PEDOT:PSS), and Buckminsterfullerene C_{60}. Device structure and direction of illumination in ITO/CuPc/C_{60}/Al (a) and ITO/PEDOT:PSS/PPV/C_{60}/Al (b) heterolayer devices.

and interference are neglected. These effects become especially important for thin film structures, where layer thicknesses are comparable to the penetration depth of the incident light, and also in the case of a highly reflecting rear contact as, for example, in the case of the metal electrodes normally used in organic photovoltaic cells.

In this article we report on experimental results of the influence of the organic layer thicknesses, the exciton diffusion length, and possible optical interference effects on short-circuit photocurrent spectra of thin film organic photovoltaic devices. We focus on donor–acceptor heterojunction systems between the conjugated polymer poly(p-phenylene-vinylene) (PPV) and Buckminsterfullerene (C_{60}),[3,9] and between the low molecular-weight material Cu-phthalocyanine (CuPc) and C_{60}.[37] These materials have been previously investigated in similar configurations partially with different donor or acceptor materials,[1,2,38,39] however, no systematic investigations with respect to the influence of the layer thicknesses were reported. In order to estimate the exciton diffusion lengths of the absorbing donor materials from our measured photocurrent spectra we used a simple rate equation for the exciton density assuming that charge separation only occurs at the PPV/C_{60}, respectively, the CuPc/C_{60} interface.

II. EXPERIMENT

A. Device fabrication and characterization

The typical device structure and the used materials are schematically shown in Fig. 1. The two different donor–acceptor systems were in both cases sandwiched between a transparent, conducting anode [indium tin oxide (ITO)], through which the cell was illuminated, and an opaque (backreflecting) Al counterelectrode. We used commercially available glass substrates coated with ITO (Flachglas, 20 $\Omega/\square$), which were cleaned with different solvents in an ultrasonic bath followed by an oxygen plasma treatment in order to enhance the work function of ITO and to improve

wetability for the aqueous solution of poly(3,4-ethylene-dioxythiophene):poly(styrenesulfonate) (PEDOT:PSS) in the case of PPV/C_{60} cells.

Thin films of PPV were obtained by spin coating the soluble tetrahydrothiophenium precursor[40,41] and subsequent thermal conversion (at 180 °C for 2 h under vacuum). By changing the concentration of the PPV-precursor solution we achieved a systematic variation of the layer thicknesses in the range of 20–150 nm. The PPV/C_{60} system consisted of an additional PEDOT:PPS layer ($\approx$25 nm) between the ITO anode and PPV [see Fig. 1(b)]. This polyelectrolyte (Baytron P, purchased from Bayer AG) was used due to the fact that in devices with PEDOT:PSS the photocurrent is improved[42–45] and current–voltage characteristics do not show leakage even for very thin PPV layer thicknesses <50 nm as compared to devices without PEDOT:PSS. The C_{60} layer in the PPV/C_{60} bilayer system was evaporated on top of the polymer under high vacuum conditions ($<1\times10^{-6}$ mbar) with a mean evaporation rate of $\approx$0.1 nm/s. The CuPc/C_{60} donor–acceptor systems were built-up by evaporation of both the CuPc and the C_{60} layer under the same high vacuum conditions and also with a mean evaporation rate of $\approx$0.1 nm/s. A systematic variation of the layer thicknesses was performed by preparing up to six devices with different thickness in only one vacuum cycle in order to obtain the same preparation conditions for comparable investigations. After evaporation of the fullerene layer in both donor–acceptor systems the metal cathode (aluminum) was evaporated under high vacuum conditions in the same vacuum cycle as the organics. By a shadow mask four independent contacts each with an area of $\approx$14 mm^2 were obtained on one substrate. In order to minimize aging effects (e.g., by oxygen or moisture), devices were stored inside a glove-box system with nitrogen atmosphere after preparation and between measurements.

For the device characterization, especially for the photocurrent spectroscopy and for the current–voltage characteristics under illumination, a 150 W xenon arc lamp served as a source of white light. This white light passed through a Bentham monochromator in order to obtain monochromatic light which was then focused onto the entrance window of the cryostat. In our experiments, we used a blazed grating in the monochromator, ruled with 1200 lines/mm, together with appropriate long-pass filters to cover the whole visible spectral range (380–780 nm). Measurements of short-circuit photocurrents of the different devices were performed with a Keithley 6517 electrometer during illumination with monochromatic light through the transparent ITO anode. The intensity of the light was measured separately using a calibrated silicon photodiode placed at the same position as the samples. For the current–voltage characteristics (I–V characteristics) in the dark and under white light illumination (without passing through the monochromator) we used a Keithley 236 source-measure unit. All photoelectric measurements were performed at room temperature under high vacuum conditions to prevent the devices from photo-oxidation. Optical absorption spectra were measured on films deposited on quartz glass substrates with a Perkin–Elmer Lambda2 UV/vis-spectrometer.
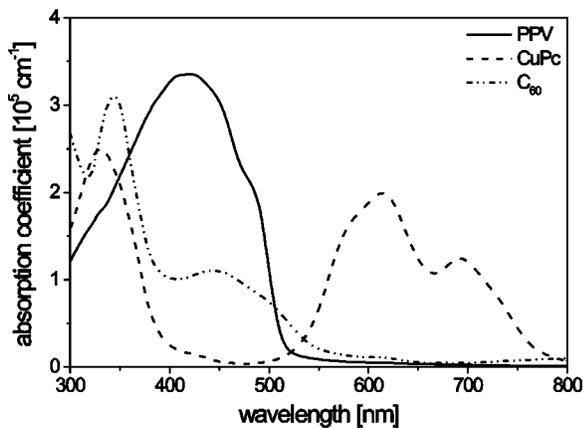
FIG. 2. Absorption spectra of poly(p-phenylenevinylene) (PPV), Cu-phthalocyanine (CuPc), and Buckminsterfullerene C_{60} in thin films. CuPc and C_{60} show complementary absorption spectra in the visible spectral range.

Before correcting the wavelength-dependent illumination intensity we verified that there was a linear dependence of the photocurrent on the intensity of the incident light ($J_{photo} \propto I_0^{\tau}$) for all our studied devices with $\tau = 1$. The light intensity dependence of the photocurrent as described by the value of the exponent τ is related to the efficiency of exciton generation and dissociation and the electrical characteristics of the photovoltaic cell. With $\tau = 1$ bimolecular recombination can be neglected and therefore all photocurrent spectra could easily be normalized to a constant light intensity of 140 $\mu W/cm^2$ for monochromatic illumination.

B. Optical absorption spectra

The different absorption spectra of the used materials are shown in Fig. 2. The absorption coefficients were obtained on films with layer thicknesses of ≈ 50 nm comparable to the thicknesses in the photovoltaic devices. PPV shows a broad absorption band in the high energy range of the visible spectrum with an absorption peak at $\lambda = 420$ nm and an absorption edge at $\lambda = 520$ nm leading to an optical band gap of 2.4 eV. Because of the lack of absorption in the long wavelength range (550–780 nm) PPV is not very suitable for white light applications over the whole visible spectrum and especially not for the air mass 1.5 solar spectrum. The absorption coefficient at the absorption peak of PPV is very high ($\alpha_{max} \approx 3.3 \times 10^5$ cm^{-1}) resulting in a short penetration depth of only $d_{min} \approx 30$ nm. So even at very thin layer thicknesses $d \leq d_{min}$ there is still considerable light absorption in PPV making thin film photovoltaic devices possible.

CuPc shows high absorption in the long wavelength range ($\alpha_{max} \approx 2 \times 10^5$ cm^{-1} at $\lambda = 620$ nm) and hardly any absorption in the short wavelength range of the visible spectrum between the two absorption edges at $\lambda = 390$ and 500 nm. The corresponding penetration depth $d_{min} \approx 50$ nm at the wavelength of the absorption peak in the low wavelength range also permits the investigation of thin CuPc layers with $d \leq 50$ nm. However, the main absorption peak appears in the UV with $\alpha_{max} \approx 2.5 \times 10^5$ cm^{-1} at $\lambda = 330$ nm, which is not very favorable for sunlight applications.

In the long wavelength range ($\lambda \geq 550$ nm) C_{60} shows almost no absorption but high absorption in the ultraviolet range. A significant contribution to the absorption spectrum also occurs in the short wavelength range with an absorption maximum at $\lambda = 440$ nm ($\alpha_{max} \approx 1.1 \times 10^5$ cm^{-1}).

For PPV/C_{60} there is a significant overlap of the absorption spectra in the short wavelength range (380–550 nm) and a very weak absorption of both materials in the long wavelength range. By contrast, in the CuPc/C_{60} bilayer system CuPc and C_{60} have nearly nonoverlapping but complementary absorption spectra in the whole visible spectral range. Therefore we can distinguish between light absorption in the CuPc layer and in the C_{60} layer by choosing the adequate wavelength, making it possible to investigate separately effects like exciton generation and diffusion in the absorbing material or optical interference. Therefore the CuPc/C_{60} heterolayer device is the more favorable system to be systematically investigated in comparison with the PPV/C_{60} system with its overlapping absorption spectra.

III. RESULTS AND DISCUSSION

For organic single layer photovoltaic devices, the relationship between the photocurrent and absorption spectra can be classified into two types: symbatic and antibatic response.[34] In the former case the photocurrent spectrum correlates well with the absorption spectrum, so that the maximum photocurrent is obtained at the wavelength of the strongest absorption. In the latter case, there is a local minimum of the photocurrent at maximum absorption and the maxima of the photocurrent spectrum occur for photon energies near the absorption edge. In single layer devices with one ohmic and one Schottky contact antibatic behavior typically occurs for illumination through the ohmic contact and symbatic response for illumination through the Schottky contact.[34,35] In this case the main exciton dissociation takes place at the Schottky contact due to the high internal field in the vicinity of the electrode.

The typical symbatic–antibatic transition can be observed by increasing the layer thickness of the organic semiconductor material from very thin layers comparable to the penetration depth ($d \leq d_{min}$) to very thick layers ($d \gg d_{min}$) resulting in thickness-dependent photocurrent spectra.

A. Thickness dependence of photocurrent spectra

In the following experiments we used bilayer systems with C_{60} in order to locate the main exciton dissociation at the donor–acceptor interface due to the photoinduced electron transfer. The additional fullerene layer does not change the distance between the illuminated ITO electrode and the dissociation interface but improves the photon-to-electron conversion efficiency not only in PPV/C_{60} systems but also in CuPc/C_{60} systems as compared to the respective single layer devices with the same donor layer thicknesses.

In the two donor–acceptor systems PPV/C_{60} and CuPc/C_{60} we systematically varied the layer thicknesses of each donor layer (PPV, CuPc) at a constant C_{60} layer thickness and of the C_{60} layer thickness at constant donor layer thicknesses in order to investigate the influence of the different layers separately.
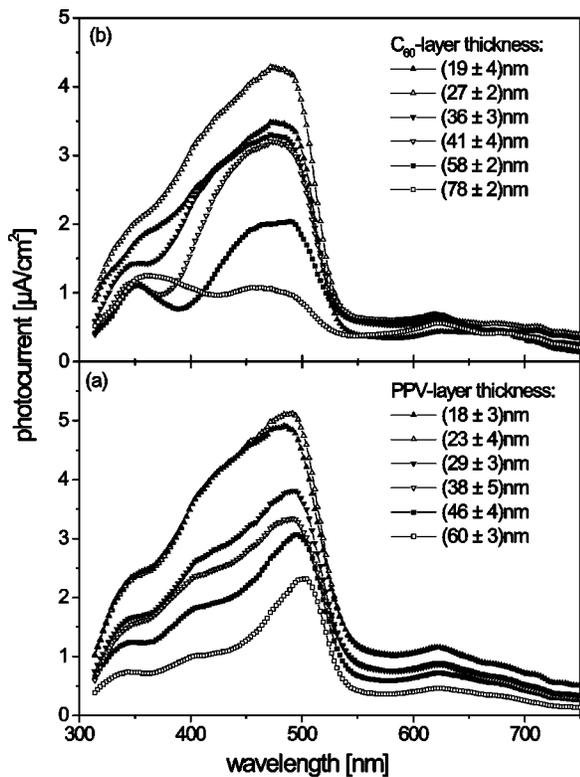
FIG. 3. Photocurrent spectra of ITO/PEDOT:PSS(25 nm)/PPV/C_{60}/Al heterolayer devices. (a) Variation of the PPV layer thickness at a fixed C_{60} layer thickness of (38±4) nm and (b) variation of the C_{60} layer thickness at a fixed PPV layer thickness of (24±4) nm.

FIG. 4. Photocurrent spectra of ITO/CuPu/C_{60}/Al heterolayer devices. (a) Variation of the CuPc layer thickness at a fixed C_{60} layer thickness of (38±4) nm and (b) variation of the C_{60} layer thickness at a fixed CuPc layer thickness of (57±4) nm.

First the PPV/C_{60} donor–acceptor system was investigated with the variation of the PPV layer thickness. In Fig. 3(a) the photocurrent spectra for different PPV layer thicknesses are shown. The C_{60} layer thickness was kept constant at (38±4) nm in all cases. The typical transition from symbatic to antibatic behavior can be seen with increasing PPV layer thickness. The photocurrent peak shifts towards longer wavelengths with increasing donor layer thickness and the photocurrent spectra no longer correlate with the absorption spectra of PPV. There is a maximum photocurrent for a PPV layer thickness of (23±4) nm, which is slightly lower than the penetration depth of PPV. With increasing PPV layer thickness the photocurrent response becomes more antibatic similar to single layer devices with a PPV/Al-Schottky contact. There is also a small contribution from the C_{60} layer to the photocurrent at short wavelengths ($\lambda = 350$ nm) and in the long wavelength range ($\lambda = 620$ nm).

In a second experiment with a PPV donor layer thickness of (24±4) nm, we systematically varied the C_{60} layer thickness. The results of the photocurrent spectra can be seen in Fig. 3(b). With increasing C_{60} layer thickness the shape of the main photocurrent peak does not change significantly. There is a maximum peak value for a C_{60} layer thickness of (27±2) nm. The photocurrent spectra clearly exhibit the contribution of C_{60} with increasing layer thickness in the short wavelength range at $\lambda = 350$ nm. The optimum C_{60} layer thickness can be a result of an optical interference between incident light and light backreflected at the Al electrode. However, due to overlapping absorption spectra (see Fig. 2)

we cannot distinguish between the influence of PPV and C_{60}.

Therefore our investigations were mainly focused on the CuPc/C_{60} donor–acceptor system. First the variation of the CuPc layer thickness for a fixed C_{60} layer thickness is investigated. There are two main contributions to the photocurrent in the CuPc/C_{60} bilayer system as can be seen in Fig. 4(a). The first one in the long wavelength range (550–780 nm) is due to absorption in the CuPc layer. A second contribution to the photocurrent spectra is found in the wavelength range of negligible CuPc absorption between 400 and 500 nm. In this range the C_{60} absorption is high and exciton generation occurs in the bulk of C_{60}. In order to achieve such a significant photocurrent contribution an efficient dissociation mechanism at the donor–acceptor interface is required. This can be achieved by a hole transfer from generated excitons in C_{60} to the highest occupied molecular orbital (HOMO) of CuPc. There is also the typical transition from symbatic to antibatic response of the photocurrent spectra with increasing CuPc layer thickness in the long wavelength range (550–780 nm), the region of bare CuPc absorption. For thin CuPc layers $d < 80$ nm the photocurrent maximum occurs at the wavelength of the absorption peak. At thicker CuPc layers this photocurrent maximum turns into a local minimum representing the antibatic response. Further there is a global maxi-

mum of the photocurrent for a CuPc layer thickness of (58±6) nm. In the wavelength region of bare C_{60} absorption there is no significant change of the shape of the photocurrent contribution with increasing CuPc layer thickness.

Through the variation of the C_{60} layer thickness from (19±5) nm to (133±7) nm at a constant CuPc donor layer thickness of (57±4) nm we obtained significant changes in the photocurrent spectra in the whole visible spectral range [see Fig. 4(b)]. In the range of CuPc absorption (550–780 nm) the photocurrent first increases with increasing C_{60} layer thickness, then reaches a maximum photocurrent at the wavelength of the absorption peak for a C_{60} layer thickness of (74±5) nm and afterwards decreases with further increase of the C_{60} layer thickness until it starts to increase again around 600 nm for the thickest C_{60} layer. Because of the constant CuPc layer thickness no transition from symbatic to antibatic response is visible. At shorter wavelengths (400–500 nm) there is an equivalent behavior, but the global maximum is already reached at a thinner C_{60} thickness of (44±4) nm, which means that the optimum C_{60} layer thickness is dependent on the wavelength of the incident monochromatic light. There is also a continuous redshift of the photocurrent peak in the short wavelength range, which is repeating periodically with increasing C_{60} layer thickness. These changes of the shape and magnitude of the photocurrent spectra indicate an optical interference effect at the dissociation interface leading to periodically modulated photocurrent spectra. In order to prove this effect we rearranged the obtained data in order to get a more detailed impression of this effect in the following section.

B. Interference effect

In order to prove the occurrence of the optical interference effect at the dissociation interface, the obtained photocurrents are plotted versus the C_{60} layer thickness for different wavelengths in Fig. 5. A periodic modulation of the photocurrent with the C_{60} layer thickness with increasing period for larger wavelengths can be seen. The lines in Fig. 5 are fit curves using a simple interference model which will be discussed below and where C_{60} absorption is neglected.

The light intensity at the dissociation interface is strongly influenced by optical interference effects due to the reflecting Al backcontact, which is the most dominant boundary condition. By increasing the C_{60} layer thickness d also the distance between the backreflecting Al electrode and the dissociation interface is changed leading to a periodic modulation of the light intensity inside the device. The light intensity $I_1(d,\lambda)$ at the donor–acceptor interface is given by the following equation (only light propagation perpendicular to the substrate plane is considered):

$$I_1(d,\lambda)=I_0(\lambda)\sin^2[k(\lambda)d-\varphi(\lambda)]$$

with

$$k(\lambda)=\frac{2\pi n(\lambda)}{\lambda}. \tag{1}$$
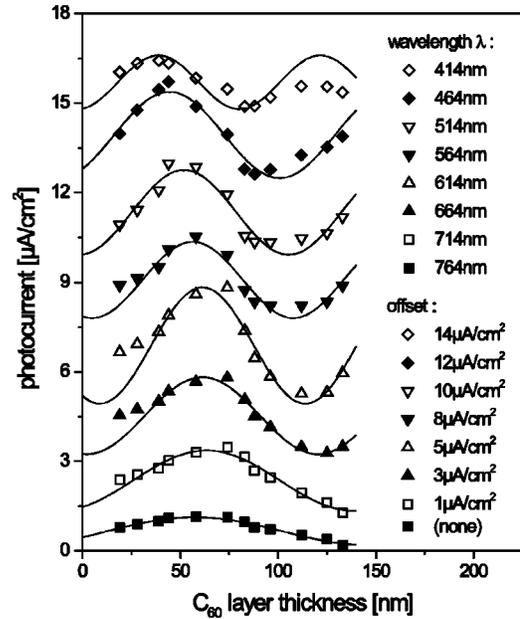
FIG. 5. Dependence of the photocurrent on the C_{60} layer thickness at a fixed wavelength in ITO/CuPc/C_{60}/Al heterolayer devices. Data are taken from Fig. 4(b).

Therein $I_0(\lambda)$ is the intensity of incident monochromatic light (after passing the CuPc layer), $k(\lambda)$ the wave vector in C_{60}, $n(\lambda)$ the refractive index of C_{60}, and $\varphi(\lambda)$ a phase shift.

Equation (1) is only correct if C_{60} absorption is negligible. The additional phase shift $\varphi(\lambda)$ is introduced to allow for a possible shift of the active zone away from the CuPc/C_{60} interface, which can occur when the exciton diffusion length in one of the materials is in the same range as the layer thickness. In this case excitons generated away from the dissociation interface also contribute to the photocurrent leading to a shift of the effective interface position. It has been found that $\varphi\approx0$ in the wavelength range of C_{60} absorption and $\varphi<0$ for CuPc absorption, which indicates a relatively large exciton diffusion length in CuPc (to be discussed in the next section). On the other hand the possibility of a finite penetration depth of the light waves into the metal electrodes in the range of a few nanometers can also shift the nodes of the standing light waves.

Fits of Eq. (1) to the observed periodic modulation of the photocurrent are shown as lines in Fig. 5. The obtained refractive index of C_{60} is about (2.5±0.3) in the wavelength range 400–650 nm and about (2.0±0.3) above this range, which is comparable to literature data.[20,46] The drop at about 650 nm can be ascribed to a slight decrease of C_{60} absorption at about the same wavelength (see Fig. 2).

A problem with the simple interference model given by Eq. (1) appears at short wavelengths and for thick C_{60} layers. In the short wavelength range C_{60} absorption is sufficiently high leading to exciton generation in C_{60} and a non-negligible photocurrent contribution as mentioned above. Thus the simple interference model has to be modified by additional terms including absorption $\alpha(\lambda)$ and exciton generation $c(\lambda)$ in the C_{60} layer. The light intensity at the dissociation interface is then given by
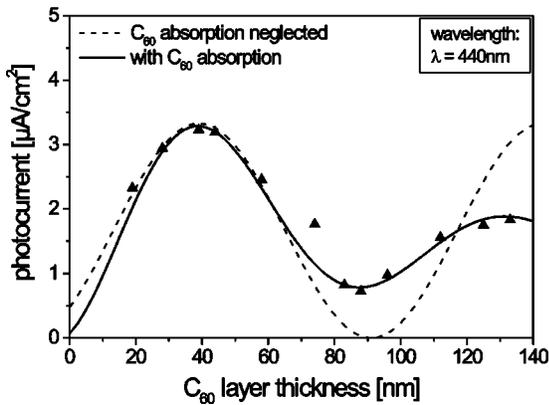
FIG. 6. Interference effect in the ITO/CuPc/C_{60}/Al heterolayer device: comparison of measured data with the interference model once including and once neglecting the additional C_{60} contribution.

$$I_2(d,\lambda) = I_1(d,\lambda)\exp[-\alpha(\lambda)d] + c(\lambda)$$
$$\times [1 - \exp(-\alpha(\lambda)d)]. \quad (2)$$

The result for the modified model is shown in Fig. 6 for a wavelength of 440 nm (region of strong C_{60} absorption). The exponential decay of the photocurrent due to C_{60} absorption [first term in Eq. (2)] is clearly seen together with an increasing offset of the photocurrent for thicker C_{60} layers [second term in Eq. (2)], which saturates for infinite C_{60} layer thickness at a value of $\approx I_0(\lambda)/4$.

As can be seen in Fig. 5 the maximum value of the photocurrent occurs at the first maximum of the periodic modulation with increasing C_{60} layer thickness and is therefore dependent on the wavelength of the incident monochromatic light. By choosing the corresponding thickness the photocurrent efficiency of the device could be maximized under monochromatic light illumination. For the whole visible spectral range and white light illumination, however, the best C_{60} layer thickness must include both main contributions to the photocurrent and should be in the range of 40–60 nm.

The predicted optimum (35 nm) and worst (80 nm) C_{60} layer thickness calculated for a polymer/C_{60} heterostructure by Pettersson et al.[20] show good agreement with our experimental results at the corresponding wavelength ($\lambda = 460$ nm, see Figs. 5 and 6). Becker et al.[47] reported that nonradiative energy transfer is important for distances $d \leqslant (90/n)$ nm from the metal electrode (n: refractive index). In our case, however, we have found no evidence for exciton quenching due to the Al-metal cathode even for thin C_{60} layers ($d < 40$ nm) since the photocurrent modulation can be simply described by optical interference. The optimum layer thickness is therefore not influenced by quenching effects of the metal electrode, at least for the investigated C_{60} layer thickness above 20 nm.

C. Exciton generation and diffusion

In Sec. III A we have shown that for the variation of the PPV or CuPc donor layer thickness at a constant C_{60} layer thickness a typical transition from symbatic response for the photocurrent spectra for thin layers to an antibatic response

for thick donor layers occurs. As seen in Figs. 3(a) and 4(a) there is a global maximum of the photocurrent at a PPV layer thickness of (23 ± 4) nm and at a CuPc layer thickness of (58 ± 6) nm in the visible spectral range. We will now analyze this behavior in more detail. Furthermore we will show that the optimum layer thicknesses allow us to estimate the exciton diffusion length in the respective material by using a simple exciton diffusion equation.

Several theoretical models have already been developed to relate the photocurrent response to the absorption spectrum. However, their assumptions are different regarding the nature of the initially photoexcited species and the mechanisms of charge generation and transport. In the paper of Harrison et al.[34] the different models developed by Ghosh et al.,[35] Tang and Albrecht,[33] DeVore,[36] Ghosh and Feng,[4] and Désormeaux et al.[32] were thoroughly discussed. Although in a qualitative sense, all of these models offer an intuitively reasonable description of the experimental results at room temperature and since the models predict very similar photocurrent responses, it is extremely difficult to distinguish between whether charge carriers are generated directly as a result of photoexcitation (intrinsic photogeneration), or indirectly by interaction of photoexcited excitons with impurities, defects, traps, and interfaces (extrinsic photogeneration). The latter is predominantly the case for single layer devices with the exciton dissociation at the organic/metal interface.

In the used heterolayer devices with C_{60} as an electron acceptor it is obvious that the main exciton dissociation mechanism is the ultrafast photoinduced charge transfer[22] at the donor–acceptor interface. Our model in principle is a mixture of the models of Ghosh and Feng,[4] Tang and Albrecht,[33] and Désormeaux[32] where the charge carrier diffusion is described by the standard diffusion equation. However, in our case we do not describe the diffusion of generated charge carriers, but the diffusion of generated neutral excitons in the bulk of the absorbing material.[20,27,48] Further on, our model is extended to take into account the photoinduced electron transfer at the donor–acceptor interface within the thin film structure. Further assumptions in our model are that (1) the absorbing layer is semi-infinite, so that far away from the illuminated electrode all light is absorbed and optical interference effects cannot occur. (2) There is no contribution to the photocurrent spectra from possible exciton dissociation in the bulk, i.e., no intrinsic dissociation. (3) Effects of reabsorption of fluorescent light, which has been shown to have a non-negligible influence on the spatial exciton distribution in molecular single crystals,[49] are not taken into consideration in this model because they only play a minor role in these devices. In the case of PPV, which has a photoluminescence (PL) efficiency of about 15%–20%, there is a fairly large spectral redshift of the PL with respect to the absorption spectrum so that reabsorption should not play a major role. In the case of CuPc the PL is much weaker so that reabsorption effects are negligible. (4) Bimolecular recombination does not occur, and finally (5) all generated charges are contributing to the steady state photocurrent, i.e., no trapping of charges occurs inside the device.

Starting from the continuity equation for neutral excitons and additional terms for exciton generation and exciton recombination the time-dependent exciton diffusion equation becomes:[34,50]

$$\frac{\partial n_{exc}(x,t)}{\partial t} = g\,\alpha N_0(t)(1-R)e^{-\alpha x} - \frac{n_{exc}(x,t)}{\tau_{exc}}$$
$$+ D_{exc}\frac{\partial^2 n_{exc}(x,t)}{\partial x^2} - F(x-x_{int})n_{exc}(x,t).$$

$$(3)$$

In Eq. (3) the time-dependent exciton density n_{exc} is described by four different terms all dependent on x, which is the distance from the illuminated ITO electrode into the bulk of the absorbing material. The first one represents the exciton generation with the number of incident photons $N_0(t)$ and the internal photon-to-exciton efficiency g. Because of reflectivity losses at the glass substrate an additional term $(1-R)$ is included. The exciton generation term is mainly determined by the exponential decay of the light intensity in the absorbing layer. The second term represents exciton recombination with a recombination lifetime τ_{exc}. The exciton diffusion is expressed by the third term with the exciton diffusion constant D_{exc}. The last term on the right-hand side of Eq. (3) stands for exciton dissociation at the donor–acceptor interface (x_{int}) with the dissociation rate $F(x-x_{int})$.

The time-dependent differential equation for the exciton density n_{exc} [Eq. (3)] is solved for stationary illumination $(\partial n_{exc}/\partial t = 0)$ and with the boundary conditions $n_{exc}(x=0) = 0$ (drain of excitons at the illuminated ITO electrode) and $n_{exc}(x\rightarrow\infty) = 0$ (no exciton creation far away in the bulk, because all light is absorbed before) by

$$n_{exc}(x) = \frac{gN_0(1-R)}{D_{exc}}\frac{\alpha L^2}{1-(\alpha L)^2}(e^{-\alpha x} - e^{-(x/L)}).\qquad(4)$$

(The latter boundary condition has to be changed if the donor layer thickness is of the same magnitude as the penetration depth and if another organic layer or a metal interface is involved.) Therein L is the exciton diffusion length defined as

$$L = \sqrt{D_{exc}\tau_{exc}}.\qquad(5)$$

This expression [Eq. (4)] gives the exciton density in the bulk of the absorbing material without exciton dissociation at the donor–acceptor interface. Similar exciton concentration profiles are reported elsewhere.[48,50,51] We note that while it is generally accepted that metal electrodes completely quench the excitons in their vicinity this process has not yet been directly proven for ITO. However, there is evidence that photoluminescence (and thus excitons) are quenched in a range of 20–25 nm from the ITO electrode,[47,52] so the assumption of an exciton sink[20] as the boundary condition may be justifiable.

Figure 7 shows exciton density profiles according to Eq. (4) for different parameter values of L and α. The maximum exciton density always occurs at a distance x_{max} from the illuminated ITO electrode given by
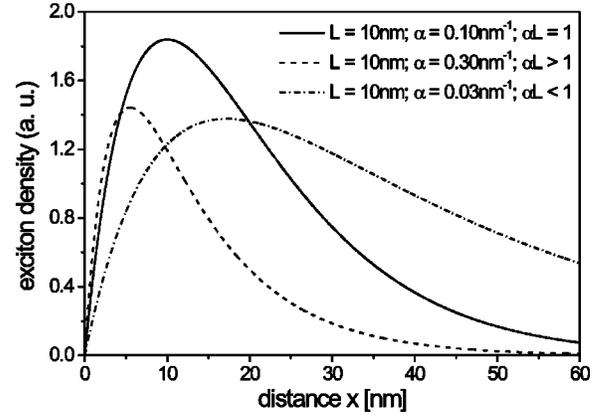
FIG. 7. Exciton density in the bulk of the absorbing material versus distance x from the illuminated ITO electrode for different values of α and L.

$$x_{max} = \frac{L\ln(\alpha L)}{\alpha L - 1}.\qquad(6)$$

This position of the maximum exciton density x_{max} is only dependent on the exciton diffusion length L and the absorption coefficient α of the absorbing material. For the special case of $\alpha L = 1$ the maximum exciton density is obtained at $x_{max} = L$ and its value is highest as compared to other combinations of α and L. Therefore the exciton diffusion length L is an important quantity that determines the optimum thickness of the absorbing layer.

The exciton dissociation processes at donor–acceptor interfaces or at metal–organic interfaces, respectively, lead to a slight modification of the exciton density model with an additional rate term for the strongly located exciton dissociation, which is only significant at or in the vicinity of the specific interface, especially at a donor–acceptor interface studied here (dissociation in the bulk region is neglected).

An important guideline for the fabrication of donor–acceptor heterolayer devices is to place the exciton dissociation interface right at the position of the maximum of the exciton density, where the highest amount of excitons is located. This means that the optimum layer thickness of the donor material is then equal to the distance x_{max} from the illuminated ITO electrode given by Eq. (6) and is therefore only dependent on the two material parameters α and L. With this equation we can plot the position of the maximum exciton density x_{max} versus the exciton diffusion length L (see Fig. 8) in order to estimate the values of L for PPV and CuPc. This relationship is shown in Fig. 8 for $\alpha = 2 \times 10^5$ cm^{-1} corresponding to the photocurrent maximum in the PPV/C$_{60}$ system at $\lambda = 480$ nm and in the CuPc/C$_{60}$ system at $\lambda = 620$ nm. From the experimentally obtained optimum layer thicknesses of PPV and CuPc (see Sec. III A) we estimate the corresponding exciton diffusion lengths to $L_{PPV} = (12\pm3)$ nm and $L_{CuPc} = (68\pm20)$ nm. The error estimates result from the limited number of investigated layer thicknesses and, especially in the case of CuPc, the large spacing between different layer thicknesses. The reproducibility of the photocurrent values in different experiments is much better than these error estimates. [The fact that the photocurrent spectra of CuPc/C$_{60}$ devices of two independent
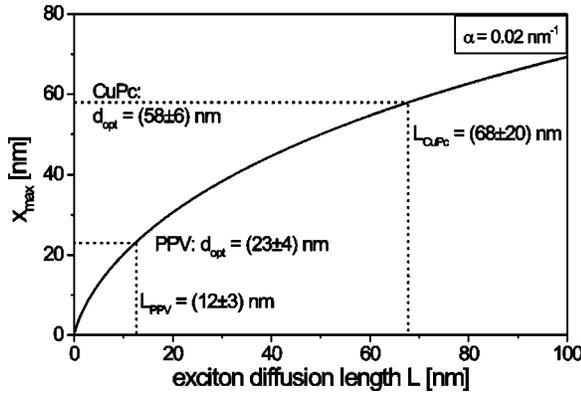
FIG. 8. Dependence of the position of maximum exciton density on the exciton diffusion length. With the optimum layer thicknesses $d_{opt} = x_{max}$ of the absorbing donor materials received from the measured photocurrent spectra [Figs. 3(a) and 4(a)] the corresponding exciton diffusion length L for PPV and CuPc is estimated.

FIG. 9. IPCE in PPV/C_{60} and CuPc/C_{60} heterolayer devices for various layer thicknesses of the absorbing donor materials.

evaporation processes perfectly match in the case of the interference effect (see Sec. III B) clearly demonstrates the high reproducibility in these cells.] The obtained values of the exciton diffusion length are comparable to literature data for oligo-PPV[47,53] and PPV,[9,54] respectively, and for different metal-phthalocyanines.[50,55] Although this is only a rough estimation of L it shows that the optimum donor layer thickness is mainly determined by the exciton diffusion length L of the material.

With these numbers it is possible to simulate the photocurrent spectra for different donor layer thicknesses qualitatively yielding the typical symbatic–antibatic transition with increasing layer thickness of the absorbing material. However, due to several unknown wavelength-dependent quantities, like g or R, which can change the shape of the photocurrent spectra, and the presence of the interference effect we are not able to calculate quantitative photocurrent spectra. Further factors to be considered are the electric transport behavior of the organic layers and the question if the separated charge carriers are driven by drift processes (due to the built-in field caused by different work functions of the electrodes) or by diffusion processes (due to the gradient of the carrier density at the interface). Therefore a quantitative device modeling requires further studies of these related issues.

D. Photovoltaic efficiency

The efficiency of a photovoltaic device can be described by the incident monochromatic photon-to-current efficiency (IPCE), which gives the ratio between the number of generated charge carriers contributing to the photocurrent and the number of incident photons. The IPCE is given as

$$\text{IPCE}[\%] = 124 \frac{|J_{sc}|[\mu\text{A/cm}^2]}{\lambda[\text{nm}] \times I_0[\text{mW/cm}^2]}, \tag{7}$$

where J_{sc} is the short-circuit photocurrent, and I_0 and λ are the intensity and the wavelength, respectively, of the incident light.

The obtained IPCE values for the PPV/C_{60} and the CuPc/C_{60} donor–acceptor system with variation of the absorbing donor layer thickness are shown in Fig. 9. The ob-

tained values represent the maximum IPCE of each spectrum, which is achieved at different wavelengths as a consequence of spectral shifts due to the symbatic–antibatic transition. The maximum IPCE value in the PPV/C_{60} system is about 10% and in CuPc/C_{60} about 3%.
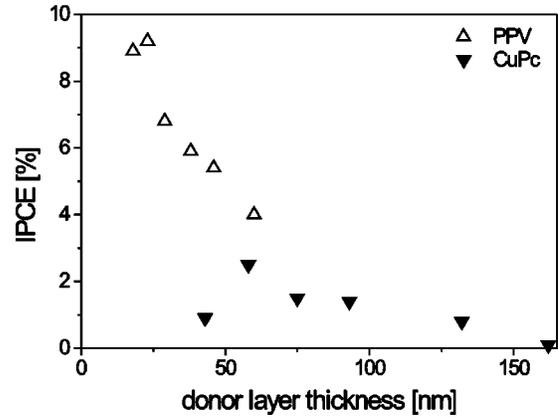
Apart from the photocurrent spectra, current–voltage characteristics are necessary to obtain the most important photovoltaic quantities, like filling factor FF or power conversion efficiency η_P, which are defined by Eq. (8) including the open circuit voltage V_{oc} and the short-circuit photocurrent J_{sc}:

$$\text{FF} = \frac{|(V \times J)|_{max}}{|V_{oc} \times J_{sc}|} \quad \text{and} \quad \eta_P = \frac{|\text{FF} \times V_{oc} \times J_{sc}|}{I_0}. \tag{8}$$

In Fig. 10 the $I–V$ characteristics in the dark and under white light illumination are shown for a typical CuPc/C_{60} bilayer system in a semilogarithmic plot. There is a low reverse current and a high rectifying behavior in the dark. Upon illumination the current for negative applied voltages changes significantly due to the high photocurrent contribution leading also to a nonzero, positive open circuit voltage V_{oc}.

More information can be obtained from a linear plot of the $I–V$ characteristics in the fourth quadrant. This is shown in Fig. 11 for white light illumination with I_0
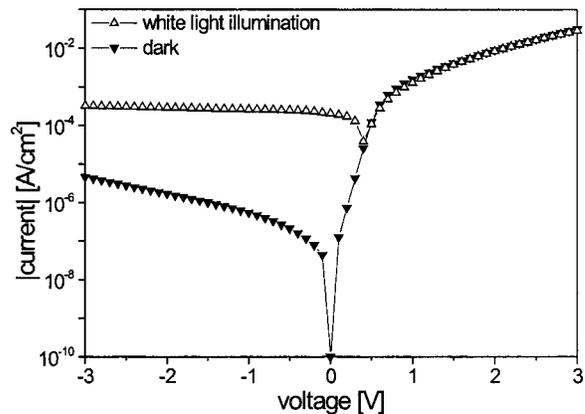
FIG. 10. $I–V$ characteristics in the dark and under white light illumination in an ITO/CuPc(57 nm)/C_{60}(83 nm)/Al bilayer device.
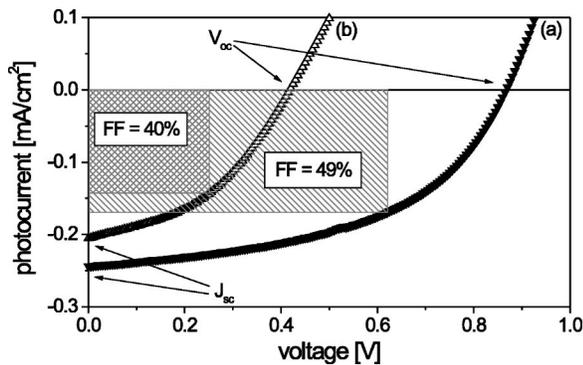
FIG. 11. $I-V$ characteristics under white light illumination for a PPV(24 nm)/C_{60}(19 nm) (a) and a CuPc(57 nm)/C_{60}(19 nm) (b) bilayer device with optimized donor layer thicknesses.

=18 mW/cm^2 for the PPV/C_{60} and CuPc/C_{60} bilayer system with optimized donor layer thicknesses. The short circuit photocurrent and the filling factor are comparable for both systems, but the open circuit voltage V_{oc} in the PPV/C_{60} system is more than twice as large as in the CuPc/C_{60} system.

In Fig. 12 the power conversion efficiency η_P versus short-circuit photocurrent J_{sc} under the same illumination conditions is shown for both donor–acceptor systems. The data were obtained from the variation of the C_{60} layer thickness as discussed before in Sec. III A. As a results, which is not shown, the open circuit voltage is independent of the C_{60} layer thickness. η_P is therefore proportional to J_{sc} and hence proportional to the quantum efficiency IPCE. This means that the higher values of V_{oc} and IPCE automatically lead to a higher power efficiency for PPV/C_{60}. Figure 12 shows that by optimizing the C_{60} thickness a considerable increase of the power efficiency to values exceeding 0.5% in PPV/C_{60} and about 0.2% in CuPc/C_{60} can be achieved even with simple bilayer devices.

IV. CONCLUSION

We have investigated the influence of light absorption, exciton diffusion, and optical interference on organic photovoltaic devices in a bilayer donor–acceptor heterojunction configuration. Assuming that charge carrier separation mainly takes place at the donor–acceptor interface due to a photoinduced electron and hole transfer, we were able to investigate the influence of the specific position of this dissociation interface on the short-circuit photocurrent spectra of PPV/C_{60} and CuPc/C_{60} systems through the variation of the individual layer thicknesses. The advantages of complementary absorption spectra of CuPc and C_{60} allowed us to distinguish between an interference effect due to standing light waves in the C_{60} layer and exciton generation and diffusion in the CuPc layer separately. From the variation of the C_{60} layer we obtained an optimum thickness of this layer between 40 and 60 nm depending on the illumination wavelength. The typical transition from symbatic to antibatic response, leading to the optical filter effect, is obtained by increasing the absorbing CuPc layer thickness. From a simple exciton density model we derived that the optimum layer thickness of the absorbing material is mainly determined by the exciton diffusion length L. From the obtained optimum donor layer thicknesses we estimated the exciton diffusion lengths in CuPc [$L_{CuPc}=(68\pm20)$ nm] and in PPV [$L_{PPV}=(12\pm3)$ nm], respectively. Power conversion efficiencies $\eta_P > 0.5\%$ were achieved with optimized donor layer thicknesses under white light illumination at 18 mW/cm^2.

[1] C. W. Tang, Appl. Phys. Lett. **48**, 183 (1986).
[2] D. Wöhrle and D. Meissner, Adv. Mater. **3**, 129 (1991).
[3] N. S. Sariciftci, D. Braun, C. Zhang, V. I. Srdanov, A. J. Heeger, G. Stucky, and F. Wudl, Appl. Phys. Lett. **62**, 585 (1993).
[4] A. K. Ghosh and T. Feng, J. Appl. Phys. **49**, 5982 (1978).
[5] H. Antoniadis, B. R. Hsieh, M. A. Abkowitz, S. A. Jenekhe, and M. Stolka, Synth. Met. **62**, 265 (1994).
[6] R. N. Marks, J. J. M. Halls, D. D. C. Bradley, R. H. Friend, and A. B. Holmes, J. Phys.: Condens. Matter **6**, 1379 (1994).
[7] G. Yu, C. Zhang, and A. J. Heeger, Appl. Phys. Lett. **64**, 1540 (1994).
[8] G. Yu and A. J. Heeger, J. Appl. Phys. **78**, 4510 (1995).
[9] J. J. M. Halls, K. Pichler, R. H. Friend, S. Moratti, and A. B. Holmes, Appl. Phys. Lett. **68**, 3120 (1996).
[10] M. Granström, K. Petritsch, A. C. Arias, A. Lux, M. R. Andersson, and R. Friend, Nature (London) **395**, 257 (1998).
[11] C. J. Brabec, F. Padinger, N. S. Sariciftci, and J. C. Hummelen, J. Appl. Phys. **85**, 6866 (1999).
[12] G. Yu, G. Srdanov, J. Wang, H. Wang, Y. Cao, and A. J. Heeger, Synth. Met. **111-112**, 133 (2000).
[13] D. Godovsky, L. Chen, L. Pettersson, O. Inganäs, M. Andersson, and J. Hummelen, Adv. Mater. Opt. Electron. **10**, 47 (2000).
[14] J. Schön, C. Kloc, E. Bucher, and B. Batlogg, Synth. Met. **115**, 177 (2000).
[15] C. Brabec, N. Sariciftci, and J. Hummelen, Adv. Funct. Mater. **11**, 15 (2001).
[16] S. Shaheen, C. Brabec, N. Sariciftci, F. Padinger, T. Fromherz, and J. Hummelen, Appl. Phys. Lett. **78**, 841 (2001).
[17] D. Vacar, E. S. Maniloff, D. W. McBranch, and A. J. Heeger, Phys. Rev. B **56**, 4573 (1997).
[18] K. Feldrapp, W. Brütting, M. Schwoerer, M. Brettreich, and A. Hirsch, Synth. Met. **101**, 156 (1999).

FIG. 12. Power efficiency versus short circuit photocurrent under white light illumination for PPV/C_{60} and CuPc/C_{60} cells with different C_{60} layer thicknesses as given in Figs. 3(b) and 4(b).

[19] J. J. M. Halls, K. Pichler, R. H. Friend, S. C. Moratti, and A. B. Holmes, Synth. Met. **77**, 277 (1996).

[20] L. A. A. Pettersson, L. S. Roman, and O. Inganäs, J. Appl. Phys. **86**, 487 (1999).

[21] C. H. Lee, G. Yu, D. Moses, and A. J. Heeger, Phys. Rev. B **49**, 2396 (1994).

[22] N. S. Sariciftci, L. Smilowitz, A. J. Heeger, and F. Wudl, Science **258**, 1474 (1992).

[23] B. Kraabel, D. McBranch, N. S. Sariciftci, D. Moses, and A. J. Heeger, Phys. Rev. B **50**, 18543 (1994).

[24] J. Bruening and B. Friedman, J. Chem. Phys. **106**, 9634 (1997).

[25] V. Dyakonov, G. Zoriniants, M. Scharber, C. J. Brabec, R. A. J. Janssen, J. C. Hummelen, and N. S. Sariciftci, Phys. Rev. B **59**, 8019 (1999).

[26] X. Wei, Z. V. Vardeny, N. S. Sariciftci, and A. J. Heeger, Phys. Rev. B **53**, 2187 (1996).

[27] M. Theander, A. Yartsev, D. Zigmantas, V. Sundström, W. Mammo, M. R. Andersson, and O. Inganäs, Phys. Rev. B **61**, 12957 (2000).

[28] E. Lebedev, T. Dittrich, V. Petrova-Koch, S. Karg, and W. Brütting, Appl. Phys. Lett. **71**, 2686 (1997).

[29] Z. Bao, A. J. Lovinger, and A. Dodabalapur, Appl. Phys. Lett. **69**, 3066 (1996).

[30] P. W. M. Blom, M. J. M. de Jong, and J. J. M. Vleggaar, Appl. Phys. Lett. **68**, 3308 (1996).

[31] G. Priebe, B. Pietzak, and R. Könenkamp, Appl. Phys. Lett. **71**, 2160 (1997).

[32] A. Désormeaux, J. J. Max, and R. M. Leblanc, J. Phys. Chem. **97**, 6670 (1993).

[33] C. W. Tang and A. C. Albrecht, J. Chem. Phys. **62**, 2139 (1975).

[34] M. G. Harrison, J. Grüner, and G. C. W. Spencer, Phys. Rev. B **55**, 7831 (1997).

[35] A. K. Ghosh, D. L. Morel, T. Feng, R. F. Shaw, and C. R. Rowe, Jr., J. Appl. Phys. **45**, 230 (1974).

[36] H. B. DeVore, Phys. Rev. **102**, 86 (1956).

[37] C. Schlebusch, B. Kessler, S. Cramm, and W. Eberhardt, Synth. Met. **77**, 151 (1996).

[38] J. Simon and J. J. André, *Molecular Semiconductors* (Springer, Berlin, 1985).

[39] K. Murata, S. Ito, K. Takahashi, and B. M. Hoffman, Appl. Phys. Lett. **68**, 427 (1996).

[40] M. Herold, J. Gmeiner, and M. Schwoerer, Acta Polym. **45**, 392 (1994).

[41] M. Herold, Ph.D. thesis, Universität Bayreuth, 1997.

[42] A. C. Arias, M. Granström, D. S. Thomas, K. Petritsch, and R. H. Friend, Phys. Rev. B **60**, 1854 (1999).

[43] J. S. Kim, M. Granström, R. H. Friend, N. Johansson, W. R. Salaneck, R. Daik, W. J. Feast, and F. Cacialli, J. Appl. Phys. **84**, 6859 (1998).

[44] L. S. Roman, M. R. Andersson, T. Yohannes, and O. Inganäs, Adv. Mater. **9**, 1164 (1997).

[45] T. M. Brown, J. S. Kim, R. H. Friend, F. Cacialli, R. Daik, and W. J. Feast, Synth. Met. **111-112**, 285 (2000).

[46] M. K. Kelly, P. Etchegoin, D. Fuchs, W. Krätschmer, and K. Fostiropoulos, Phys. Rev. B **46**, 4963 (1992).

[47] H. Becker, S. E. Burns, and R. H. Friend, Phys. Rev. B **56**, 1893 (1997).

[48] N. Karl, A. Bauer, J. Holzäpfel, J. Marktanner, M. Möbius, and F. Stölzle, Mol. Cryst. Liq. Cryst. **252**, 243 (1994).

[49] J. Kalinowski, J. Godlewski, and J. Gliński, Acta Phys. Pol. A **65**, 413 (1984).

[50] H. R. Kerp, H. Donker, R. B. M. Koehorst, T. J. Schaafsma, and E. E. van Faassen, Chem. Phys. Lett. **298**, 302 (1998).

[51] H. R. Kerp and E. E. van Faassen, Phys. Chem. Chem. Phys. **1**, 1761 (1999).

[52] S. Saito, T. Tsutsui, M. Era, N. Takada, E.-I. Aminaka, and T. Wakimoto, Mol. Cryst. Liq. Cryst. **253**, 125 (1994).

[53] A. Haugeneder, M. Neges, C. Kallinger, W. Spirkl, U. Lemmer, J. Feldmann, U. Scherf, E. Harth, A. Gügel, and K. Müllen, Phys. Rev. B **59**, 15346 (1999).

[54] J. J. M. Halls and R. H. Friend, Synth. Met. **85**, 1307 (1997).

[55] C. C. Leznoff and A. B. P. Lever, *Phthalocyanines-Properties and Applications* (VCH, New York, 1996), Vol. 4.